

# **SOFT X-RAYS AND EXTREME ULTRAVIOLET RADIATION**

---

*Principles and Applications*

**DAVID ATTWOOD**

UNIVERSITY OF CALIFORNIA, BERKELEY  
AND  
LAWRENCE BERKELEY  
NATIONAL LABORATORY



**CAMBRIDGE**  
UNIVERSITY PRESS

PUBLISHED BY THE PRESS SYNDICATE OF THE UNIVERSITY OF CAMBRIDGE  
The Pitt Building, Trumpington Street, Cambridge, United Kingdom

CAMBRIDGE UNIVERSITY PRESS

The Edinburgh Building, Cambridge CB2 2RU, UK      www.cup.cam.ac.uk

40 West 20th Street, New York, NY 10011-4211, USA      www.cup.org

10 Stamford Road, Oakleigh, Melbourne 3166, Australia

Ruiz de Alarcón 13, 28014 Madrid, Spain

© Cambridge University Press 1999

This book is in copyright. Subject to statutory exception  
and to the provisions of relevant collective licensing agreements,  
no reproduction of any part may take place without  
the written permission of Cambridge University Press.

First published 2000

Printed in the United States of America

*Typeface* Times Roman 10/12 pt.    *System* L<sup>A</sup>T<sub>E</sub>X 2<sub>ε</sub> [TB]

*A catalog record for this book is available from  
the British Library.*

*Library of Congress Cataloging-in-Publication Data*

Attwood, David T.

Soft x-rays and extreme ultraviolet radiation : principles and  
applications / David Attwood.

p. cm.

Includes bibliographical references.

ISBN 0-521-65214-6 (hbk.)

1. Grenz rays. 2. Ultraviolet radiation. I. Title.

QC482.G68A88 1999

539.7'222 – dc21

99-21078

CIP

ISBN 0 521 65214 6 hardback

# Contents

---

<b>PREFACE</b>	<i>page</i> xiii
<b>ACKNOWLEDGMENTS</b>	xv
<b>CHAPTER 1. INTRODUCTION</b>	1
1.1 The Soft X-Ray and Extreme Ultraviolet Regions of the Electromagnetic Spectrum	1
1.2 Basic Absorption and Emission Processes	5
1.3 Atomic Energy Levels and Allowed Transitions	10
1.4 Scattering, Diffraction, and Refraction of Electromagnetic Radiation	18
References	21
Homework Problems	23
<b>CHAPTER 2. RADIATION AND SCATTERING AT EUV AND SOFT X-RAY WAVELENGTHS</b>	24
2.1 Maxwell's Equations and the Wave Equation	24
2.2 Calculating Scattered Fields	27
2.3 Radiated Power and Poynting's Theorem	33
2.4 Scattering Cross Sections	38
2.5 Scattering by a Free Electron	39
2.6 Scattering by Bound Electrons	41
2.7 Scattering by a Multi-electron Atom	44
References	53
Homework Problems	54
<b>CHAPTER 3. WAVE PROPAGATION AND REFRACTIVE INDEX AT EUV AND SOFT X-RAY WAVELENGTHS</b>	55
3.1 The Wave Equation and Refractive Index	56
3.2 Phase Variation and Absorption of Propagating Waves	61
3.3 Reflection and Refraction at an Interface	66
3.4 Total External Reflection of Soft X-Rays and EUV Radiation	69

3.5	Reflection Coefficients at an Interface	71
3.5.1	$\mathbf{E}_0$ Perpendicular to the Plane of Incidence	71
3.5.2	$\mathbf{E}_0$ Parallel to the Plane of Incidence	77
3.6	Brewster's Angle	80
3.7	Field Penetration into a Lossy Medium Near the Critical Angle	82
3.8	Determination of $\delta$ and $\beta$ : The Kramers–Kronig Relations	90
3.9	Applications to Glancing Incidence Optics	94
3.10	Enhanced Reflectivity from Periodic Structures	95
	References	96
	Homework Problems	97
	<b>CHAPTER 4. MULTILAYER INTERFERENCE COATINGS</b>	98
4.1	Introduction	98
4.2	Constructive Interference of Scattered Radiation	99
4.3	Computational Model for Calculating Reflection from a Multilayer Mirror	103
4.4	Multilayer Fabrication	106
4.5	Applications of Multilayer Coated Optics	107
4.5.1	Soft X-Ray and Extreme Ultraviolet Photoemission Microscopy for Surface Science	108
4.5.2	Extreme Ultraviolet and Soft X-Ray Astronomy	108
4.5.3	Extreme Ultraviolet Lithography	110
4.5.4	Plasma Diagnostics	113
4.5.5	Polarization Studies of Magnetic Materials	114
4.5.6	The X-Ray Microprobe	116
	References	119
	Homework Problems	122
	<b>CHAPTER 5. SYNCHROTRON RADIATION</b>	123
5.1	Introduction	124
5.2	Characteristics of Bending Magnet Radiation	126
5.3	Characteristics of Undulator Radiation	135
5.3.1	Undulator Radiation Pattern	137
5.3.2	The Central Radiation Cone	139
5.4	Undulator Radiation: Calculations of Radiated Power, Brightness, and Harmonics	141
5.4.1	The Undulator Equation	141
5.4.2	Comments on Undulator Harmonics	146
5.4.3	Power Radiated in the Central Radiation Cone	147
5.4.4	Power as a Function of Angle and Total Radiated Power	156
5.4.5	Spectral Bandwidth of Undulator Radiation	161
5.4.6	Spectral Brightness of Undulator Radiation	165
5.4.7	Time Structure	168
5.4.8	Polarization Properties of Undulator Radiation	170
5.5	The Scale of Harmonic Motion	172

5.6	The Transition from Undulator to Wiggler Radiation	177
5.7	Wiggler Power and Flux	182
5.8	Femtosecond Pulse Generation	185
	References	186
	Homework Problems	188
<b>CHAPTER 6. PHYSICS OF HOT DENSE PLASMAS</b>		189
6.1	Introduction	190
6.2	Short and Long Range Interactions in Plasmas	191
6.3	Basic Parameters for Describing a Plasma	195
6.4	Microscopic, Kinetic, and Fluid Descriptions of a Plasma	197
6.4.1	The Microscopic Description	197
6.4.2	The Kinetic Description	200
6.4.3	The Fluid Description	202
6.4.4	Plasma Expansion	211
6.4.5	Electron-Acoustic Waves	213
6.4.6	Ion-Acoustic Waves	217
6.4.7	Transverse Electromagnetic Waves in a Plasma	219
6.4.8	Resonance Absorption	227
6.4.9	Waves in a Magnetized Plasma	227
6.4.10	Non-linear Processes in a Plasma	227
6.4.11	Threshold for Non-linear Processes	232
6.5	Numerical Simulations	234
6.5.1	Particle in Cell Simulations	234
6.5.2	Langrangian Zonal Calculations of Plasma Mass and Energy Transport	236
6.6	Density Gradients: UV and EUV Probing	238
6.7	X-Ray Emission from a Hot Dense Plasma	241
6.7.1	Continuum Radiation and Blackbody Spectra	242
6.7.2	Line Emission and Ionization Bottlenecks	246
6.7.3	Sub-kilovolt Line and Continuum Emissions	248
6.7.4	Multi-kilovolt Line Emission	254
6.7.5	Suprathermal X-Rays	256
6.7.6	Laser Wavelength Trends	257
6.8	High Harmonic Generation with Femtosecond Laser Pulses	259
	References	261
	Homework Problems	266
<b>CHAPTER 7. EXTREME ULTRAVIOLET AND SOFT X-RAY LASERS</b>		267
7.1	Basic Processes	268
7.2	Gain	274
7.3	Recombination Lasing with Hydrogen-like Carbon Ions	279
7.4	Collisionally Pumped Neon-like and Nickel-like Lasers	283
7.5	Compact EUV Lasers	291

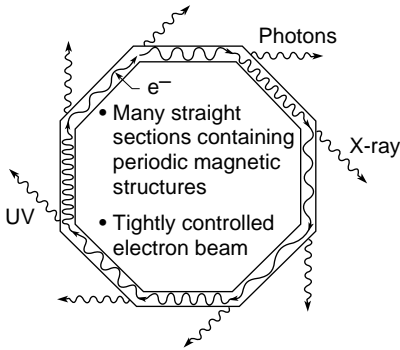
References	295
Homework Problems	299
<b>CHAPTER 8. COHERENCE AT SHORT WAVELENGTHS</b>	<b>300</b>
8.1 Concepts of Spatial and Temporal Coherence	301
8.2 Examples of Experiments that Require Coherence	306
8.3 Spatial and Spectral Filtering	309
8.4 Spatial and Spectral Filtering of Undulator Radiation	310
8.5 Spatially Coherent EUV and Soft X-Ray Lasers	318
8.6 The Van Cittert–Zernike Theorem	321
8.7 Examples of High Contrast Fringes Formed at Short Wavelengths	330
References	333
Homework Problems	336
<b>CHAPTER 9. SOFT X-RAY MICROSCOPY WITH DIFFRACTIVE OPTICS</b>	<b>337</b>
9.1 Introduction	338
9.2 The Fresnel Zone Plate Lens	342
9.3 Diffraction of Radiation by Pinhole Apertures and Zone Plates	349
9.3.1 Pinhole Aperture	351
9.3.2 Zone Plate	353
9.4 Spatial Resolution of a Zone Plate Lens	357
9.5 Depth of Focus and Spectral Bandwidth	361
9.6 Spatial Resolution Beyond the Rayleigh Limit: The Effective Angular Illumination Profile	363
9.7 High Resolution Soft X-Ray Microscopy	365
9.7.1 The Soft X-Ray Microscope	366
9.7.2 The Scanning Soft X-Ray Microscope	367
9.8 Applications to the Life Sciences	369
9.8.1 Biological Applications of the Soft X-Ray Microscope	372
9.8.2 Biological Applications of the Scanning Soft X-Ray Microscope	377
9.9 Applications to the Physical Sciences: Analytic Tools for Materials and Surface Science at Spatial Resolutions Below 100 Nanometers	379
9.10 Zone Plate Fabrication	385
References	388
Homework Problems	394
<b>CHAPTER 10. EXTREME ULTRAVIOLET AND X-RAY LITHOGRAPHY</b>	<b>395</b>
10.1 Deep Ultraviolet (DUV) Lithography and Beyond	396
10.2 Extreme Ultraviolet (EUV) Lithography	404
10.3 X-Ray Proximity Lithography	408
References	412
Homework Problems	416

---

<b>APPENDIX A. UNITS AND PHYSICAL CONSTANTS</b>	417
A.1 The International System of Units (SI)	417
A.2 Physical Constants	419
References	419
<b>APPENDIX B. ELECTRON BINDING ENERGIES, PRINCIPAL K- AND L-SHELL EMISSION LINES, AND AUGER ELECTRON ENERGIES</b>	420
References	427
<b>APPENDIX C. ATOMIC SCATTERING FACTORS, ATOMIC ABSORPTION COEFFICIENTS, AND SUBSHELL PHOTOIONIZATION CROSS-SECTIONS</b>	428
References	439
<b>APPENDIX D. MATHEMATICAL AND VECTOR RELATIONSHIPS</b>	440
D.1 Vector and Tensor Formulas	440
D.2 Series Expansions	441
D.3 Trigonometric Relationships	442
D.4 Definite Integrals	443
D.5 Functions of a Complex Variable	444
D.6 Fourier Transforms	447
D.7 The Dirac Delta Function	447
D.8 The Cauchy Principal Value Theorem	447
References	448
<b>APPENDIX E. SOME INTEGRATIONS IN <math>k, \omega</math>-SPACE</b>	449
<b>APPENDIX F. LORENTZ SPACE-TIME TRANSFORMATIONS</b>	454
F.1 Frequency and Wavenumber Relations	456
F.2 Angular Transformations	458
F.3 The Lorentz Contraction of Length	460
F.4 Time Dilation	460
F.5 Transforming $dP'/d\Omega'$ to $dP/d\Omega$	461
References	464
<b>INDEX</b>	465

# Chapter 5

# SYNCHROTRON RADIATION



### Bending Magnet:

$$\hbar\omega_c = \frac{3e\hbar B\gamma^2}{2m} \quad (5.7)$$

### Wiggler:

$$\hbar\omega_c = \frac{3e\hbar B\gamma^2}{2m}$$

$$n_c = \frac{3K}{4} \left( 1 + \frac{K^2}{2} \right)$$

$$P_T = \frac{\pi e K^2 \gamma^2 I N}{3\epsilon_0 \lambda_u}$$

### Undulator:

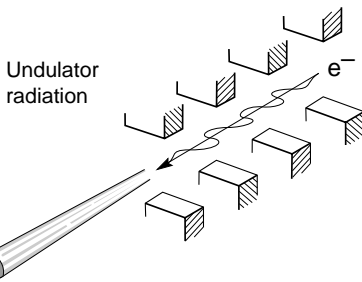
$$\lambda = \frac{\lambda_u}{2\gamma^2} \left( 1 + \frac{K^2}{2} + \gamma^2 \theta^2 \right) \quad (5.28)$$

$$K = \frac{eB_0\lambda_u}{2\pi mc} \quad (5.18)$$

$$\theta_{\text{cen}} = \frac{1}{\gamma^* \sqrt{N}} \quad (5.15)$$

$$\left. \frac{\Delta\lambda}{\lambda} \right|_{\text{cen}} = \frac{1}{N} \quad (5.14)$$

$$\bar{P}_{\text{cen}} = \frac{\pi e \gamma^2 I}{\epsilon_0 \lambda_u} \frac{K^2}{\left( 1 + \frac{K^2}{2} \right)^2} f(K) \quad (5.41)$$



(see Colorplate X)

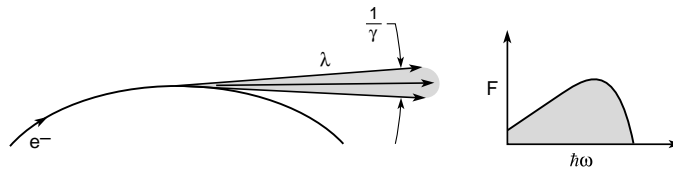


**FIGURE 5.1.** Bending magnet radiation occurs when a relativistic electron travels in a uniform magnetic field, executing a circular motion with acceleration directed toward the center. The radiation is directed tangentially outward in a narrow radiation cone, giving the appearance of a sweeping “searchlight.” The radiation spectrum is very broad, analogous to a “white light” x-ray light bulb. The emission angle is typically  $1/\gamma$ , where  $\gamma$  is the Lorentz contraction factor.

In this chapter we briefly review the central features of synchrotron radiation, beginning with estimates of radiated photon energies and angular divergence based on the application of well-known results from the theory of relativity and Heisenberg’s uncertainty principle. For bending magnet radiation, formulae describing photon flux as a function of angle and photon energy are summarized in a convenient handbook style. Undulator radiation, generated by relativistic electrons traversing a periodic magnet structure, is calculated in detail. The approach taken makes maximal use of the well-known classical results of dipole radiation. This is accomplished by solving the electron equation of motion in the laboratory frame of reference, then making a Lorentz transformation to the frame of reference moving with the average electron velocity. In this frame of reference the motion is non-relativistic, yielding the well-known  $\sin^2 \Theta$  angular dependence of radiated power per unit solid angle. These results are then Lorentz transformed back to the laboratory (observer) frame of reference. A central radiation cone, defined as containing a  $1/N$  relative spectral bandwidth, is shown to correspond to an angular half width of  $1/\gamma\sqrt{N}$ , where  $N$  is the number of magnet periods. Power radiated in the central cone is readily calculated from the dipole formula. Calculations of spectral brightness follow in a straightforward manner. Wiggler radiation, the strong field extension of undulator radiation, is shown to be dominated by a large number of harmonics that merge to a continuum at high photon energy. The spectral shape of wiggler radiation is similar to that of bending magnetic radiation, but shifted to higher photon energy (by the higher magnetic fields) and to increased ( $2N$ ) photon flux.

## 5.1 INTRODUCTION

It is well known that an accelerated charged particle, such as one traveling on a curved trajectory, will emit radiation. When moving at relativistic speeds, this radiation is emitted as a narrow cone tangent to the path of the particle.<sup>1</sup> Synchrotron radiation is generated when relativistic electrons (or positrons) are accelerated (undergo a change of direction) in a magnetic field, as seen in Figure 5.1.

There are three types of magnetic structures commonly used to produce synchrotron radiation: bending magnets, undulators, and wigglers. Bending magnets cause a single curved trajectory as pictured in Figure 5.1. The result is a fan of radiation around the bend. Undulators are periodic magnetic structures with relatively weak magnetic fields. The periodicity causes the electron to experience a harmonic oscillation as it moves in the axial direction, resulting in a motion characterized by small angular excursions called undulations,<sup>2,3</sup> as shown in Figure 5.2. The weak magnetic fields cause the amplitude of this undulation to be small.

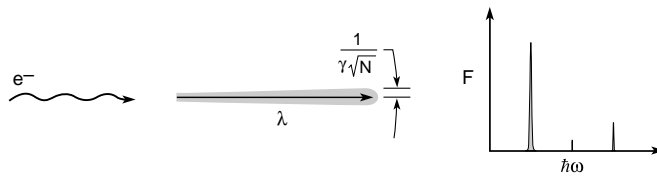


**FIGURE 5.2.** Undulator radiation is generated as a highly relativistic electron traverses a periodic magnetic field. In the undulator limit, the magnetic field is relatively weak and the resultant angular excursions of the electron are smaller than the angular width of the natural radiation cone,  $1/\gamma$ , normally associated with synchrotron radiation. The frequency spread of undulator radiation can be very narrow, and the radiation can be extremely bright and partially coherent, under certain circumstances. The characteristic emission angle is narrowed by a factor  $\sqrt{N}$ , where  $N$  is the number of magnetic periods. Typically  $N$  is of order 100. Depending on the magnet strength, harmonic radiation may be generated.

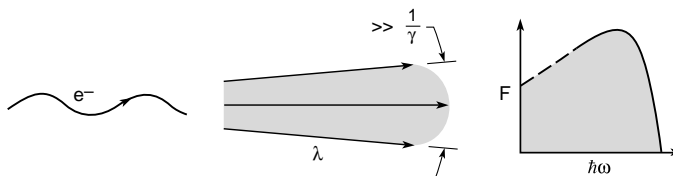


**FIGURE 5.3.** Wiggler radiation is also generated from a periodic magnet structure, but in the strong magnetic field limit where in at least one plane the angular excursions are significantly greater than the natural  $(1/\gamma)$  radiation cone. Because accelerations are stronger in this limit, the radiation generated peaks at higher photon energies and is more abundant (higher photon flux and more power). The radiation spectrum is very broad, similar to that of the bending magnet. Although more power is radiated, wiggler radiation is less bright because of the substantially increased radiation cone.

Hence, the resultant radiation cone is narrow. In combination with a tightly confined electron beam, this leads to radiation with small angular divergence and relatively narrow spectral width, properties we generally associate with the coherence properties of lasers.<sup>4</sup> W wigglers are a strong magnetic field version of undulators. Due to the stronger fields, the oscillation amplitude and concomitant radiated power is larger. The radiation cone is broader in both space and angle. The radiation spectrum is similar to that of bending magnets, but characterized by a much larger photon flux and a shift to harder x-rays (shorter wavelengths), as seen in Figure 5.3.

Historically, synchrotron radiation was first observed as energy loss in electron storage rings. Logically, the first synchrotron radiation sources for general scientific use were simple parasitic beam ports utilizing otherwise lost radiation at existing storage rings. Over time, however, sources have been constructed for dedicated use as synchrotron radiation facilities (*second generation* facilities). The newest synchrotron facilities (*third generation* facilities) are composed of many straight sections specially optimized to produce high brightness undulator and wiggler radiation. Figure 5.4 illustrates yesterday's and today's synchrotron radiation facilities.

Figure 5.5 is a simple schematic of a synchrotron radiation source. The relativistic electrons are injected into the ring from a linear accelerator and (energy) booster synchrotron. Various magnetic lenses keep the electrons traveling along the desired trajectory. Synchrotron radiation is produced as the electrons pass through the bending magnets, undulators, and

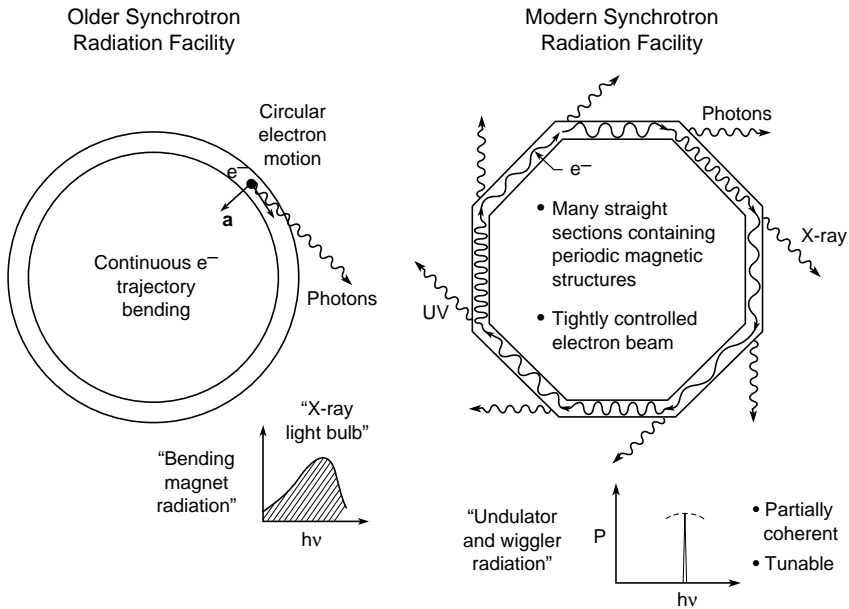


**FIGURE 5.4.** (a) Early synchrotron radiation facilities were basically circular rings for bending magnet radiation, although some have been retrofitted with periodic magnetic structures (undulators or wigglers). They generally have an electron beam of relatively large cross-section and angular divergence. (b) Modern storage rings are dedicated to broad scientific use and optimized for high spectral brightness through the inclusion of many long straight sections for undulators and wigglers, as well as very tightly confined (spatial and angular extent) electron beams. Bending magnet radiation is also generated in turning from one straight section to the next (not shown).

wigglers. Electron beam energy lost to synchrotron radiation is replenished with a radio-frequency accelerator (a cavity with an axial electric field oscillating at the frequency of arrival of sequential electron bunches). Typical parameters characterizing synchrotron radiation from two modern storage rings, one optimized for the generation of soft x-rays and one optimized for the generation of hard x-rays, are given in Table 5.1.

## 5.2 CHARACTERISTICS OF BENDING MAGNET RADIATION

In this introductory section, we wish to use simple arguments to show why one expects to see radiation at x-ray wavelengths. The arguments are based on an estimate of the time duration of the observed radiation signal and an application of Heisenberg's uncertainty principle for photon energy. Bending magnet radiation is sometimes described as a sweeping "searchlight," analogous to the headlight of a toy train on a circular track. This searchlight effect is a general manifestation associated with radiation from relativistic particles undergoing acceleration. An electron experiencing radial acceleration as it travels around a circle emits radiation through a broad angular pattern – as seen in its frame of reference. However, angular patterns are very much compressed upon Lorentz transformation from one frame of reference (that moving with the electron) to another (the laboratory frame of the observer) when the relative motion is highly relativistic. In Appendix F it is shown that angles measured from the direction of

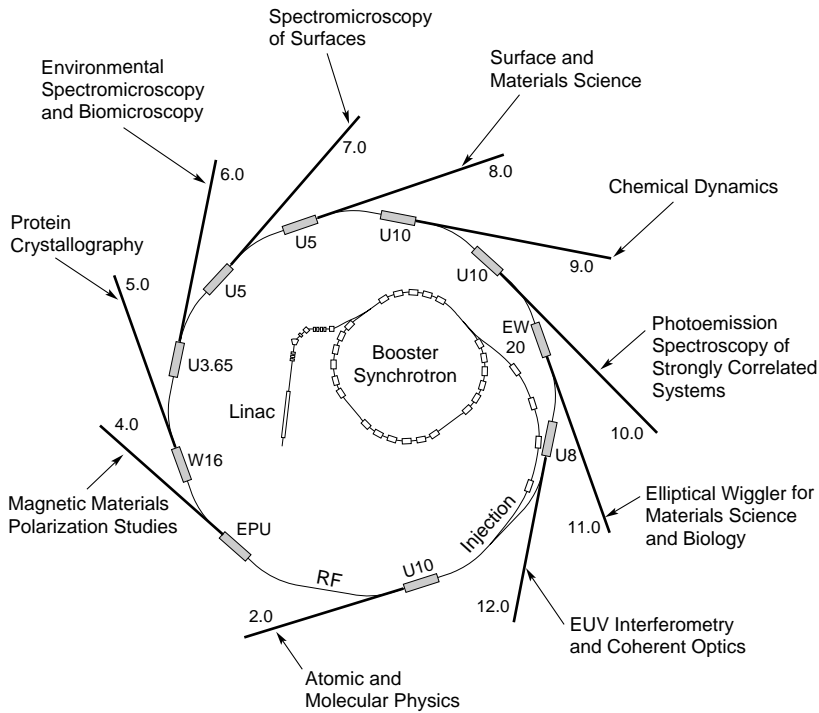


**FIGURE 5.5.** This sketch of an electron storage ring optimized for soft x-ray radiation shows a linear accelerator (linac) and booster synchrotron that bring electrons up to an energy matched to storage ring magnet settings, an injection system, which directs electrons into the ring, and a radio frequency (rf) generator to replenish the energy lost to synchrotron radiation as the electrons pass bending magnets, undulators, and wigglers. Straight sections for undulators and wigglers direct energy into beamlines and end sections for various scientific studies. Bending magnet radiation beamlines, located between straight sections, are not shown.

motion are related by

$$\tan \theta = \frac{\sin \theta'}{\gamma(\beta + \cos \theta')} \quad (5.1)$$

where  $\theta'$  is observed in the frame of reference moving with the electron,  $\theta$  is in the laboratory frame,  $\beta \equiv v/c$  (where  $v$  is the relative velocity between frames and  $c$  is the velocity of light), and  $\gamma \equiv 1/(1 - v^2/c^2)^{1/2}$ . For highly relativistic electrons  $\beta$  approaches unity, and  $\gamma \gg 1$ . Thus for arbitrarily large emission angles  $\theta'$ , in the electron frame, the radiation is folded into a narrow forward radiation cone of half angle

$$\theta \simeq \frac{1}{2\gamma} \quad (5.2)$$

leading to the description of synchrotron radiation as being concentrated in a narrow “search-light beam.”

**TABLE 5.1.** Typical parameters for synchrotron radiation at two complementary storage ring facilities. Both rings are optimized for small electron phase space (emittance) and the use of multiple straight sections for undulators and wigglers. Bending magnet radiation is obtained as the electron beam turns from one straight section to the next. The two facilities are complementary in that one is optimized for soft x-rays while the other is optimized for hard x-rays. The Advanced Light Source (ALS) is operated by Lawrence Berkeley National Laboratory in California. The Advanced Photon Source (APS) is operated by Argonne National Laboratory in Illinois. Parameters for other facilities around the world are tabulated by Winck (Ref. 5).

Facility	ALS	APS
Electron energy	1.90 GeV	7.00 GeV
$\gamma$	3720	13,700
Current (mA)	400	100
Circumference (m)	197	1100
RF frequency (MHz)	500	352
Pulse duration (FWHM) (ps)	35–100	170
<i>Bending Magnet Radiation:</i>		
Bending magnet field (T)	1.27	0.599
Critical photon energy (keV)	3.05	19.5
Critical photon wavelength	0.407 nm	0.0636 nm (0.636 Å)
Bending magnet sources	24	35
<i>Undulator Radiation:</i>		
Number of straight sections	12	40
Undulator period (typical) (cm)	5.00	3.30
Number of periods	89	72
Photon energy ( $K = 1, n = 1$ )	457 eV	9.40 keV
Photon wavelength ( $K = 1, n = 1$ )	2.71 nm	0.132 nm (1.3 Å)
Tuning range ( $n = 1$ )	2.0–5.4 nm	0.10–0.35 nm
Tuning range ( $n = 3$ )	0.68–1.8 nm	0.033–0.12 nm
Central cone half-angle ( $K = 1$ )	35 $\mu$ rad	11 $\mu$ rad
Power in central cone ( $K = 1, n = 1$ ) (W)	2.3	12
Flux in central cone (photons/s)	$3.1 \times 10^{16}$	$7.9 \times 10^{15}$
$\sigma_x, \sigma_y$ ( $\mu$ m)	260, 16	320, 50
$\sigma'_x, \sigma'_y$ ( $\mu$ rad)	23, 3.9	23, 7
Brightness ( $K = 1, n = 1$ ) <sup>a</sup> [(photons/s)/mm <sup>2</sup> · mrad <sup>2</sup> · (0.1%BW)]	$2.3 \times 10^{19}$	$4.8 \times 10^{18}$
Total power ( $K = 1, \text{all } n, \text{all } \theta$ ) (W)	187	780
Other undulator periods (cm)	3.65, 8.00, 10.0	2.70, 5.50, 12.8
<i>Wiggler Radiation:</i>		
Wiggler period (typical) (cm)	16.0	8.5
Number of periods	19	28
Magnetic field (maximum) (T)	2.1	1.0
$K$ (maximum)	32	7.9
Critical photon energy (keV)	5.1	33
Critical photon wavelength	0.24 nm	0.038 nm (0.38 Å)
Total power (max. $K$ ) (kW)	13	7.4

<sup>a</sup>Using Eq. (5.65). See comments following Eq. (5.64) for the case where  $\sigma'_{x,y} \simeq \theta_{\text{cen}}$ .

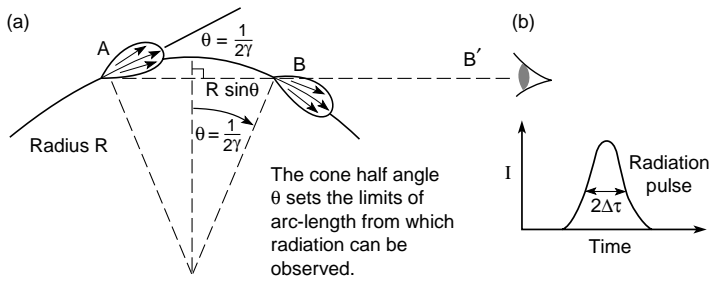


**FIGURE 5.6.** (a) A schematic of bending magnet radiation illustrating the “searchlight” effect, similar to that of the headlight of a train on a circular track, which is a general feature of radiation by highly relativistic electrons. (b) The time width of the observed radiation pulse is determined by transit time differences between radiation and electrons between points  $A$  and  $B$ . The uncertainty relationship between pulse duration and minimal spread of photon energy indicates that a broad range of photon energies, extending to the x-ray region, is to be expected. (Following Hofmann.<sup>2</sup>)

As an electron traverses a curved path, radiation is emitted tangentially, as seen in Figure 5.6, in a narrow radiation cone of half width  $\theta \simeq 1/2\gamma$ . For electrons circulating in a ring, we can estimate the photon energies and wavelengths radiated using simple arguments based on Heisenberg’s uncertainty principle,  $\Delta E \cdot \Delta \tau \geq \hbar/2$ , where  $\Delta \tau$  is the (rms) time duration during which one detects radiation, and  $\Delta E$  is the uncertainty (rms spread) in observed photon energies. We begin by estimating the detected pulse duration,  $2 \Delta \tau$ , of radiation emitted by a short bunch of electrons following a circular trajectory of radius  $R$ . We estimate the time extent of the observed signal by considering a detector at point  $B$  or equivalently further to the right at  $B'$ . As the electron comes within an angle  $\theta \simeq 1/2\gamma$  of the horizon at point  $A$ , the detector will be in the path of emitted photons. These photons will be detected after a transit time of the light,  $\tau_r$ . The signal will continue until the electron reaches point  $B$ , beyond which the radiation cone has turned too far to permit reception by our detector. The electron will reach point  $B$  after a transit time around the bend,  $\tau_e$ . The pulse width,  $\Delta \tau$ , shown in Figure 5.6(b) is the difference between these two transit times, i.e., the detector detects radiation after a time  $\tau_r$ , and stops detecting radiation at  $\tau_e$ .

Following this outline, we see that

$$2 \Delta \tau = \tau_e - \tau_r$$

$$2 \Delta \tau = \frac{\text{arc length}}{v} - \frac{\text{radiation path}}{c}$$

$$2 \Delta \tau \simeq \frac{R \cdot 2\theta}{v} - \frac{2R \sin \theta}{c}$$

Noting that  $\theta \simeq 1/2\gamma$ , making a small angle approximation for  $\sin \theta$ , and substituting  $v = \beta c$ , one obtains

$$2 \Delta \tau \simeq \frac{R}{\gamma v} - \frac{R}{\gamma c} = \frac{R}{\gamma} \left( \frac{1}{v} - \frac{1}{c} \right)$$

Writing  $v = \beta c$ , one has

$$2 \Delta \tau \simeq \frac{R}{\gamma \beta c} (1 - \beta)$$

Noting that

$$\gamma \equiv \frac{1}{\sqrt{1 - \beta^2}}$$

$$\gamma^2 = \frac{1}{1 - \beta^2} = \frac{1}{(1 - \beta)(1 + \beta)}$$

and thus for  $\beta = v/c$  approaching unity

$$1 - \beta \simeq \frac{1}{2\gamma^2} \quad (5.3)$$

the expression for the duration of the radiation pulse becomes

$$2\Delta\tau \simeq \frac{R}{2c\gamma^3} \quad (5.4a)$$

This can be expressed as an anticipated photon energy spread through the use of Heisenberg's uncertainty principle<sup>6</sup> and an expression for the radius of curvature  $R$ . From the uncertainty principle,

$$\Delta E \cdot \Delta \tau \geq \hbar/2$$

Combining this with the expression in Eq. (5.4a) for the pulse duration, we see that the photons will have an rms energy spread of order\*

$$\Delta E \geq \frac{2\hbar c \gamma^3}{R} \quad (5.4b)$$

To better appreciate the photon energies implied by Eq. (5.4b) it is useful to replace the electron radius of curvature  $R$  with an expression involving  $\gamma$  and the magnetic field. For electrons crossing a perpendicular magnetic field, as in a bending magnet, the relativistically correct form of the equation of motion can be written as

$$\mathbf{F} = \frac{d\mathbf{p}}{dt} = -e\mathbf{v} \times \mathbf{B}$$

where  $\mathbf{p} = \gamma m \mathbf{v}$  is the momentum,<sup>6</sup>  $m$  is the electron rest mass,  $\gamma$  is the Lorentz factor,  $\mathbf{v}$  is the velocity, and  $\mathbf{B}$  is the magnetic flux density. For electron motion in a uniform magnetic field, the electron energy and thus  $\gamma$  is a constant, so that only the direction of  $\mathbf{v}$  changes, not its magnitude. To see this we write the rate of change of electron energy as

$$\frac{dE_e}{dt} = \mathbf{v} \cdot \mathbf{F} = \underbrace{-e\mathbf{v} \cdot (\mathbf{v} \times \mathbf{B})}_{\equiv 0}$$

\*Similar arguments are given in J.D. Jackson (Ref. 1), First Edition, pp. 475–477.

which is zero by vector identity (see Appendix B). Thus the electron energy, which can be written<sup>6</sup> as  $\gamma mc^2$ , is a constant, viz.,

$$\frac{dE_e}{dt} = \frac{d}{dt}(\gamma mc^2) = 0$$

Thus  $\gamma$ , and therefore the scalar magnitude  $v$  of the velocity, are both constant. The equation of motion can be rewritten as

$$\gamma m \frac{d\mathbf{v}}{dt} = -e\mathbf{v} \times \mathbf{B}$$

Since the magnitude of  $\mathbf{v}$  is constant, the magnitude of the acceleration is also constant, equal to  $evB/\gamma m$ , in a plane perpendicular to  $\mathbf{B}$ . This corresponds to motion along a circle, with centripetal acceleration  $v^2/R$ , so that the scalar form of the equation of motion becomes

$$\gamma m \left( -\frac{v^2}{R} \right) = -evB$$

Solving for the radius of curvature, we have

$$R = \frac{\gamma m v}{eB}$$

or for highly relativistic electrons

$$R \simeq \frac{\gamma mc}{eB}$$

Using this in Eq. (5.4b), the rms spread of photon energies for bending magnet radiation becomes

$$\Delta E \geq \frac{2e\hbar B\gamma^2}{m} \quad (5.4c)$$

which we note depends on the electron charge to mass ratio,  $e/m$ , and the product  $B\gamma^2$ . If we substitute values for  $e$ ,  $\hbar$ , and  $m$ , Eq. (5.4c) indicates photon energies in the keV range (nanometer wavelengths) for typical values of  $\gamma$  and  $B$  found in modern storage rings, e.g.,  $\gamma$  of several thousand and  $B$  of 1T or more. For highly relativistic electrons it is convenient to express the total electron energy in terms of  $\gamma$  and the electron rest energy,  $mc^2$ , as<sup>6</sup>

$$\gamma = \frac{E_e}{mc^2} = 1957 E_e(\text{GeV}) \quad (5.5)$$

where on the right side we have used the fact that the electron rest energy is 0.5110 MeV, and expressed the electron energy  $E_e$  in GeV.

The description of expected photon energy spread obtained above, Eq. (5.4c), is based on relatively simple arguments involving Heisenberg's uncertainty principle. It is valuable in that it provides a measure of the expected photon energies radiated by accelerated charges moving at relativistic speeds, and gives a functional dependence in terms of  $B\gamma^2$ . The numerical factor (2) obtained by this argument is, however, is somewhat arbitrary in that it depends on the angular distribution of radiation embodied in our assumption that  $\theta \simeq 1/2\gamma$ . A more precise description of the photon energy distribution, obtained by a rigorous solution of Maxwell's equations for a relativistic electron in a uniform magnetic field, introduces instead a factor of  $\frac{3}{2}$  and a more useful definition of  $\Delta E$ . The results are somewhat complex, involving

**TABLE 5.2.** Sample values of the functions  $G_1(y)$  and  $H_2(y)$ , where  $y = \omega/\omega_c$  (following Green.<sup>7</sup>).

$y$	$G_1(y)$	$H_2(y)$
0.0001	$9.959 \times 10^{-2}$	$6.271 \times 10^{-3}$
0.0010	$2.131 \times 10^{-1}$	$2.910 \times 10^{-2}$
0.0100	$4.450 \times 10^{-1}$	$1.348 \times 10^{-1}$
0.1000	$8.182 \times 10^{-1}$	$6.025 \times 10^{-1}$
0.3000	$9.177 \times 10^{-1}$	$1.111 \times 10^0$
0.5000	$8.708 \times 10^{-1}$	$1.356 \times 10^0$
0.7000	$7.879 \times 10^{-1}$	$1.458 \times 10^0$
1.000	$6.514 \times 10^{-1}$	$1.454 \times 10^0$
1.500	$4.506 \times 10^{-1}$	$1.250 \times 10^0$
2.000	$3.016 \times 10^{-1}$	$9.780 \times 10^{-1}$
3.000	$1.286 \times 10^{-1}$	$5.195 \times 10^{-1}$
4.000	$5.283 \times 10^{-2}$	$2.493 \times 10^{-1}$
5.000	$2.125 \times 10^{-2}$	$1.131 \times 10^{-1}$
7.000	$3.308 \times 10^{-3}$	$2.107 \times 10^{-2}$
10.00	$1.922 \times 10^{-4}$	$1.478 \times 10^{-3}$

modified Bessel functions of the second kind (see Refs. 1–3). Defining  $\theta$  as the in-plane observation angle for radiation from relativistic electrons traveling in a circular path, and  $\psi$  as the out-of-plane (vertical) angle, Kim<sup>3</sup> shows that the photon flux  $F_B$  for bending magnet radiation is given on axis by

$$\frac{d^3 F_B}{d\theta d\psi d\omega/\omega} \Big|_{\psi=0} = 1.33 \times 10^{13} E_e^2 (\text{GeV}) I (\text{A}) H_2(E/E_c) \frac{\text{photons/s}}{\text{mrad}^2 \cdot (0.1\% \text{ BW})} \quad (5.6)$$

where the electron energy  $E_e$  is in GeV, the average current  $I$  is in amperes, where the units of relative spectral bandwidth  $d\omega/\omega$  are expressed non-dimensionally as a factor of  $10^{-3}$ , or 0.1% BW, as discussed further in section 5.4.6, and the function

$$H_2(y) = y^2 K_{2/3}^2(y/2)$$

is a modified Bessel function dependence, tabulated in Table 5.2 and shown graphically in Figure 5.7. The ratio  $E/E_c$  is the photon energy normalized with respect to a *critical photon energy*

$$E_c = \hbar\omega_c = \frac{3e\hbar B\gamma^2}{2m} \quad (5.7a)$$

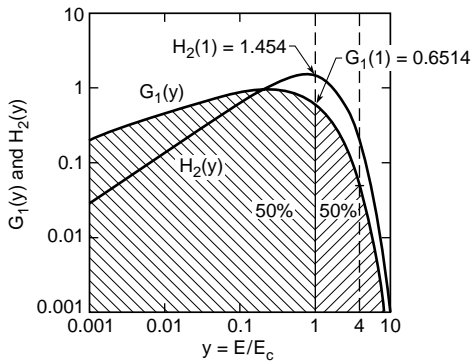


**FIGURE 5.7.** The functions  $H_2(y)$ , representing on-axis photon flux from a bending magnet, and  $G_1(y)$ , representing the vertically integrated photon flux, as functions of photon energy normalized to the critical photon energy. Half the radiated power is in photons of energy greater than  $E_c$ , and half in photons of energy less than  $E_c$  (following Kim<sup>3</sup>). Note that for a photon energy of  $4E_c$  the photon flux is reduced a factor of about 10 from its value at  $E_c$ .

The critical photon energy is that for which half the radiated power is in higher energy photons and half is in lower energy photons. As such it provides a primary parameter for characterizing bending magnet radiation.

Equation (5.7a) can be rewritten in practical units as

$$E_c(\text{keV}) = 0.6650 E_e^2(\text{GeV}) B(\text{T}) \quad (5.7b)$$

where the critical photon energy is in keV, the electron beam energy is given in GeV, and the magnetic field in teslas. The corresponding *critical wavelength* is

$$\lambda_c = \frac{4\pi mc}{3eB\gamma^2} \quad (5.7c)$$

which can be written in practical units of nanometers, GeV, and teslas as

$$\lambda_c(\text{nm}) = \frac{1.864}{E_e^2(\text{GeV}) B(\text{T})} \quad (5.7d)$$

Note that the critical photon energy given in Eq. (5.7a) is well within the range of photon energies estimated by Eq. (5.4c) on the basis of relativistic angular transformations and Heisenberg uncertainty arguments.

The critical photon energy is in fact a very useful parameter for characterizing synchrotron radiation from relativistic electrons as they traverse the fields of a bending magnet. For example, of two new storage rings operating in the United States, the Advanced Light Source (ALS) at Lawrence Berkeley Laboratory in California, with a beam energy of 1.9 GeV and a bending magnet field strength of 1.27 T, has a critical photon energy of 3.1 keV and a critical wavelength of 0.41 nm (4.1 Å), while the Advanced Photon Source (APS) at Argonne National Laboratory in Illinois, with a beam energy of 7.0 GeV and a bending magnet field strength of 0.60 T, has a critical photon energy of 20 keV and a critical wavelength of 0.064 nm (0.64 Å).

Typical parameters characterizing synchrotron radiation from these two representative facilities are presented in Table 5.1. Between the two they cover a broad region of the electromagnetic spectrum. In fact, inspection of Figure 5.7 shows that on axis the photon flux decreases by only a factor of 10 at a photon energy equal to  $4E_c$ . For many experiments this significantly extends the useful range of bending magnet radiation, for instance to 12 keV at the ALS, and to 80 keV at the APS. Further enhancements using strong field periodic wigglers are also possible. Wiggler radiation is described at the end of this chapter.

**TABLE 5.3.** Measures of angular divergence of bending magnet radiation in the vertical plane, as a function of normalized photon energy. Single sided rms and full width at half maximum (FWHM) measures are given. (Following Kim.<sup>3</sup>)

$E/E_c$	$\sigma'_\psi$ (rms)	FWHM
0.01	$5.0/\gamma$	$12/\gamma$
0.03	$3.3/\gamma$	$7.8/\gamma$
0.1	$2.0/\gamma$	$4.7/\gamma$
0.3	$1.2/\gamma$	$2.8/\gamma$
1	$0.64/\gamma$	$1.5/\gamma$
3	$0.37/\gamma$	$0.9/\gamma$
10	$0.18/\gamma$	$0.4/\gamma$

On occasion it is convenient to know the bending magnet photon flux per unit horizontal angle  $\theta$ , integrating out the vertical plane  $\phi$ -dependence. In this case Kim<sup>3</sup> finds that the radiated photon flux, in units of photons per second per milliradian per 0.1% relative spectral bandwidth, is given by

$$\frac{d^2 F_B}{d\theta d\omega/\omega} = 2.46 \times 10^{13} E_e(\text{GeV}) I(\text{A}) G_1(E/E_c) \frac{\text{photons/s}}{\text{mrad} \cdot (0.1\% \text{BW})} \quad (5.8)$$

where the function

$$G_1(y) = y \int_y^\infty K_{5/3}(y') dy'$$

is also shown graphically in Figure 5.7. Note that by the definition of  $E_c$ , the integrals of  $G_1(y)$  from zero to one and from one to infinity are equal, as suggested in Figure 5.7. Table 5.2 gives some specific values of the functions  $H_2(\omega/\omega_c)$  and  $G_1(\omega/\omega_c)$ .

Note that the bending magnet radiation is linearly polarized when viewed in the horizontal plane of acceleration. When viewed outside this plane, bending magnet radiation is elliptically polarized. The out of plane photon flux, decomposed into horizontal and vertical polarization components, is given by Kim.<sup>3</sup> Kim also introduces a convenient measure of angular divergence<sup>3</sup> in the vertical plane,  $\sigma'_\psi$ , for bending magnet radiation. This divergence angle varies with normalized photon energy,  $E/E_c$ . Fitted to a Gaussian angular distribution, the rms half angle in the vertical plane is  $0.64/\gamma$  at  $E/E_c = 1$ . Full width at half maximum (FWHM) measures are larger by a factor of 2.35. Sample values are given in Table 5.3 for sample values of  $E/E_c$ .

Since the acceleration of electrons is confined to the horizontal plane (for vertical bending magnet fields), the electric field of the resultant radiation will be linearly polarized in that

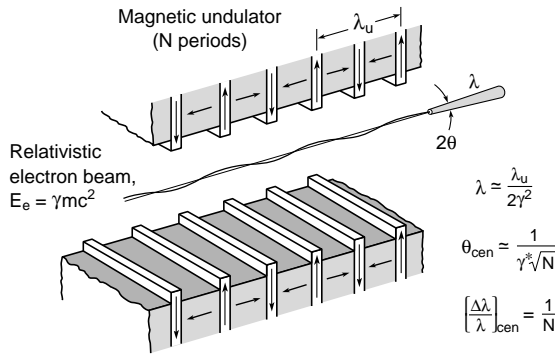


**FIGURE 5.8.** Illustration of narrow cone undulator radiation that is generated by electrons traversing a periodic magnet structure.

plane. The general polarization properties of bending magnet radiation for arbitrary angles of observations are discussed in Ref. 3.

### 5.3 CHARACTERISTICS OF UNDULATOR RADIATION

An electron traversing a periodic magnet structure<sup>8</sup> of moderate field strength will undergo a small amplitude oscillation and therefore radiate. If the electron's angular excursions are small compared to the natural radiation width,  $\theta_e < 1/2\gamma$ , the device is referred to as an *undulator* (see Figure 5.8). The resultant radiation is greatly reduced in wavelength,  $\lambda$ , from that of the magnet period,  $\lambda_u$ . We will see shortly that Lorentz contraction and relativistic Doppler shift lead to a reduction in the radiated wavelength by a factor of  $2\gamma^2$ . As  $\gamma$  can easily be several thousand, undulator periods measured in centimeters lead to observed x-ray wavelengths measured in angstroms.

While discussing undulator radiation, we will find it convenient to consider the radiation in several frames of reference. Many of the calculations will be done in the reference frame moving with the electron. We will then transform the results to the rest frame of the laboratory via Lorentz transformations (see Ref. 9 or Appendix F, Lorentz Space–Time Transformations). The following is a brief introduction to undulator radiation. A more detailed discussion will follow in subsequent sections.

In the frame moving with the electron, the electron “sees” a periodic magnet structure moving toward it with a relativistically (Lorentz) contracted period,  $\lambda'$ , given by

$$\lambda' = \frac{\lambda_u}{\gamma} \quad (5.9)$$

where  $\gamma \equiv 1/\sqrt{1 - v^2/c^2}$ ,  $v$  is the relative velocity, and  $c$  is the velocity of light in vacuum, as discussed in Appendix F. Due to the periodic magnet, the electron experiences an oscillation and consequently radiates. In the frame moving with the electron this problem is that of the classical *radiating dipole*, a point charge oscillating with an amplitude much smaller than the radiated wavelength. The frequency of this emitted radiation, in the reference frame of

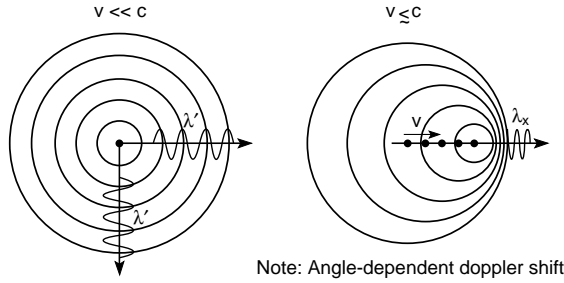


**FIGURE 5.9.** Radiation from an oscillating charge moving at (a) a non-relativistic and (b) a relativistic speed. Short wavelengths are observed because comparable speeds of the moving charge ( $v$ ) and the radiation ( $c$ ) reduce the separation of succeeding phase fronts. Indeed, as  $v$  approaches  $c$ , the spatial phase variations ( $\lambda$ ) are dramatically compressed by many orders of magnitude. (Following J. Madey.)

the electron, is

$$f' = \frac{c}{\lambda'} = \frac{c\gamma}{\lambda_u}$$

To the observer in the fixed laboratory reference frame, the radiation wavelength is further reduced by Doppler shifting. The Doppler shift is dependent on the relative velocity and therefore is dependent on the observation angle  $\theta$ , as can be deduced from Figure 5.9. The shortest wavelength is observed on axis. The relativistic form of the Doppler frequency formula is [see Appendix F, Eq. (F.8b)]

$$f = \frac{f'}{\gamma(1 - \beta \cos \theta)} = \frac{c}{\lambda_u(1 - \beta \cos \theta)} \quad (5.10)$$

where  $\beta \equiv v/c$  and  $\theta$  is the observation angle measured from the direction of motion.

Let us first analyze the observed frequency on axis. Here  $\theta = 0$ ,  $\cos \theta = 1$ , and

$$f = \frac{c}{\lambda_u(1 - \beta)}$$

As noted in Eq. (5.3), for  $\beta \simeq 1$  we have  $1 - \beta \simeq 1/2\gamma^2$ . Therefore, the observed radiation frequency on axis is

$$f = \frac{2\gamma^2 c}{\lambda_u}$$

and the observed wavelength on axis is

$$\lambda = \frac{c}{f} = \frac{\lambda_u}{2\gamma^2} \quad (5.11)$$

Note that the observed wavelength,  $\lambda$ , is relativistically contracted by a factor  $2\gamma^2$  from the period of the undulator. Again using the ALS as an example, with a 1.9 GeV electron energy,  $\gamma \simeq 3700$  [see Eq. (5.5)]; thus  $2\gamma^2 \simeq 2.8 \times 10^7$ . If the undulator period is  $\lambda_u = 5.0$  cm, the

resultant on-axis radiation will be relativistically shifted to an observed wavelength of order

$$\lambda \simeq \frac{5.0\text{cm}}{2.8 \times 10^7} \simeq 1.8 \text{ nm}$$

Thus the periodic magnet generates radiation peaked in the soft x-ray region of the electromagnetic spectrum.

If we wish to consider Doppler shifts at small angles off axis ( $\theta \neq 0$ ), we can return to Eq. (5.10) and use the small angle approximation. The Taylor expansion for small angles is  $\cos \theta = 1 - \theta^2/2 + \dots$ ; therefore,

$$f = \frac{\frac{c}{\lambda_u}}{1 - \beta \left(1 - \frac{\theta^2}{2} + \dots\right)} = \frac{\frac{c}{\lambda_u}}{1 - \beta + \frac{\beta\theta^2}{2} + \dots} = \frac{\frac{c}{(1-\beta)\lambda_u}}{1 + \frac{\beta\theta^2}{2(1-\beta)}}$$

Since  $\beta \simeq 1$  and by Eq. (3)  $1 - \beta \simeq 1/2\gamma^2$ , one has

$$f = \frac{\frac{2\gamma^2 c}{\lambda_u}}{1 + \frac{2\gamma^2\theta^2}{2} - \dots} = \frac{2c\gamma^2}{\lambda_u(1 + \gamma^2\theta^2)}$$

In terms of the observed wavelength  $\lambda = c/f$ , one has to first order

$$\lambda = \frac{\lambda_u}{2\gamma^2}(1 + \gamma^2\theta^2) \quad (5.12)$$

We again see the  $2\gamma^2$  contraction on axis, but now with the off-axis radiation having a wavelength increased by a factor  $(1 + \gamma^2\theta^2)$ . Hence, to observe the narrow bandwidth characteristic of this relativistic harmonic oscillator, it is necessary to select only near-axis radiation.

As we will see explicitly in a following section, the magnetically induced undulation causes the electron to follow a somewhat longer pathlength as it traverses the undulator. Thus, the mean axial velocity is reduced, resulting in a modified Doppler shift and therefore somewhat longer wavelengths than indicated by Eq. (5.12), and a broader radiation cone as well.

### 5.3.1 Undulator Radiation Pattern

As we saw in Chapter 2, Eqs. (2.25)–(2.33), an oscillating electron of charge  $-e$  undergoing an acceleration  $\mathbf{a}$  will radiate electromagnetic waves characterized by an electric field (also see Leighton, Ref. 9).

$$E(\mathbf{r}, t) = \frac{ea(t - r/c)}{4\pi\epsilon_0 c^2 r} \sin \Theta$$

and an orthogonal magnetic field

$$H(\mathbf{r}, t) = \frac{ea(t - r/c)}{4\pi cr} \sin \Theta$$

where  $t - r/c$  is the retarded time (delayed arrival at distance  $r$ ), and  $\Theta$  is the angle between the direction of acceleration ( $\mathbf{a}$ ) and the propagation direction ( $\mathbf{k}_0$ ). Because the electric and magnetic fields are orthogonal, their cross product gives a Poynting vector  $\mathbf{S}$  (power per

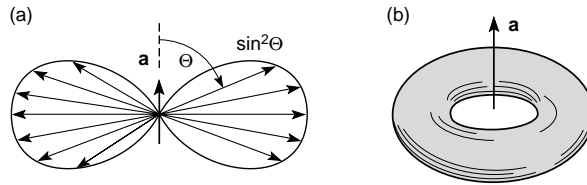


**FIGURE 5.10.** Illustration of an oscillating charge and the resultant radiation pattern. Note that there is no radiation in the direction of acceleration, giving the radiation pattern a doughnut-like appearance.

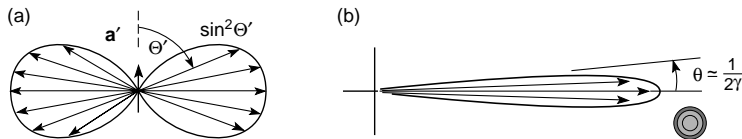


**FIGURE 5.11 (see Colorplate VI).** (a) Illustration of the radiation pattern of an oscillating electron in the frame of reference moving with the average electron speed. (b) Illustration of the radiation pattern of a highly relativistic electron as observed in the laboratory frame of reference. The shortest wavelengths are observed on axis. (Following Hofmann.<sup>2</sup>)

unit area) of

$$\mathbf{S} = \mathbf{E} \times \mathbf{H} = \left[ \frac{e^2 a^2 \sin^2 \Theta}{16\pi^2 \epsilon_0 c^3 r^2} \right] \mathbf{k}_0$$

The radiated power per unit solid angle is [Chapter 2, Eq. (2.34)]

$$\frac{dP}{d\Omega} = r^2 |\mathbf{S}| = \frac{e^2 a^2}{16\pi^2 \epsilon_0 c^3} \sin^2 \Theta$$

Hence, the radiation pattern has a toroidal  $\sin^2 \Theta$  shape, because there is no radiation in the acceleration direction ( $\Theta = 0$ ), as illustrated in Figure 5.10.

For an undulating electron, undergoing simple oscillations in its own reference frame ( $\gamma$ ), one obtains the same radiation pattern. However, the radiation pattern as observed in the laboratory frame is relativistically contracted into a narrow radiation cone (the so-called searchlight effect) as shown in Figure 5.11(b). Considering the symmetry of the problem, it is convenient to work with a polar coordinate system measured from the  $z$ -axis. For instance, in the plane defined by the electron acceleration ( $\mathbf{a}$ ) and the  $z$ -axis, the factor  $\sin^2 \Theta'$  becomes  $\cos^2 \theta'$ ,  $\theta'$  being the polar angle measured away from the  $z$ -axis in the primed coordinate system. In this primed electron frame of reference the radiation pattern has a half-intensity angle at  $\cos^2 \theta' = \frac{1}{2}$  or  $\theta' = 45^\circ$ . According to Eq. (5.1), this corresponds to an angle in the unprimed laboratory (observer) frame of reference of  $\theta \simeq 1/2\gamma$ . Returning to the example of a 1.9 GeV electron ( $\gamma \simeq 3700$ ), in this case traversing a periodic magnet structure, one anticipates that radiated x-rays will largely be confined to a cone of half angle  $140 \mu\text{rad}$ . As we will see in the following paragraphs, further cone narrowing can be obtained in the case of undulator radiation.

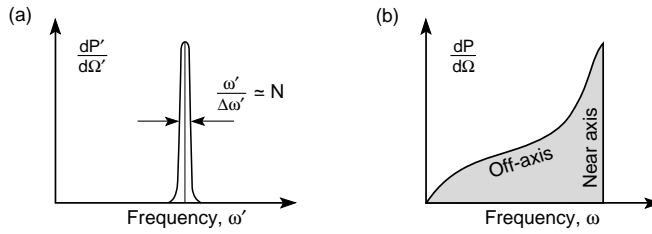


**FIGURE 5.12.** (a) The radiation spectrum as seen in the frame of reference moving with the electron is narrow with a relative spectral bandwidth of order  $1/N$ , where  $N$  is the number of oscillation periods. (b) In the laboratory frame of reference, the wavelengths are shorter, but the spectrum is broader due to off-axis Doppler effects. (Following Hofmann.<sup>2</sup>)

### 5.3.2 The Central Radiation Cone

The spectrum of radiation in the two reference frames is shown in Figure 5.12(a) and (b). Figure 5.12(a) shows the narrow spectral width in the electron frame, set by the harmonic oscillation for a fixed number of periods  $N$ . This is essentially a frequency–time (Laplace) transform.

For example, the ALS has undulators of 5.0 cm period, with a length of 89 periods, so that one can expect  $\Delta\omega'/\omega' = \Delta\lambda'/\lambda'$  of order 0.01. Note, however, that upon transformation to the laboratory frame of reference, off-axis Doppler effects will broaden this considerably. Figure 5.12(b) illustrates the Doppler shifted spectrum that results when the  $\sin^2 \Theta$  dipole radiation pattern is transformed according to Eqs. (5.1) and (5.12).

Recall that we have determined the undulator equation (5.12) in the laboratory frame, viz.,

$$\lambda \simeq \frac{\lambda_u}{2\gamma^2}(1 + \gamma^2\theta^2)$$

and have also noted that the radiation is primarily contained in a narrow cone of half angle  $\theta = 1/2\gamma$ . The corresponding spectral width within this cone can thus be estimated by taking the difference of Eq. (5.12) for two angles. Taking the wavelength as  $\lambda$  on axis ( $\theta = 0$ ), and  $\lambda + \Delta\lambda$  off axis at angle  $\theta$ , then taking ratios, one obtains

$$\frac{\Delta\lambda}{\lambda} \simeq \gamma^2\theta^2 \quad (5.13)$$

where Eq. (5.13) shows how the wavelength increases as one observes the radiation off axis. Note that for radiation within the cone of half angle  $\theta \simeq 1/2\gamma$  the relative spectral bandwidth given by Eq. (5.13) is  $\frac{1}{4}$ ; thus the cone of half-intensity half angle encloses a relative spectral bandwidth of about 25%. Use of aperture spectral filtering is illustrated in Figure 5.13. Often, further spectral narrowing is desired, for instance, when probing in the vicinity of sharp atomic resonance features. In such cases, a monochromator of some type (see Chapter 8) is employed that acts as a narrow bandpass filter. In the case of radiation from a single electron or a tightly constrained bunch of electrons, modest spectral filtering (as narrow as  $1/N$ ) can be obtained with a simple small-angle selecting aperture (pinhole). In this limit, we will see that angular width and spectral width are closely connected. The interrelationship is shown in Figure 5.14.

Further cone narrowing can be appreciated by considering the undulator equation for two angular positions, one on axis and one at angle  $\theta$ , as we did previously in Eq. (5.13). If one

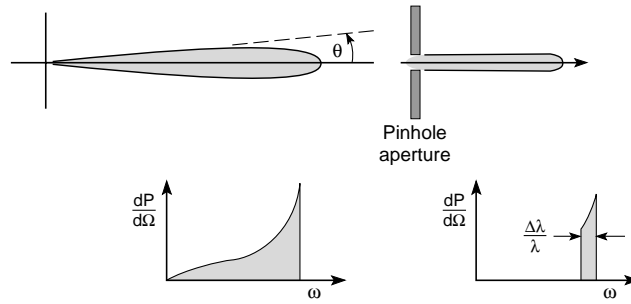


**FIGURE 5.13.** The spectrum of undulator radiation in the laboratory frame of reference before and after selecting an angular cone near the axis. With a sufficiently small electron beam phase space (size–angle product) this can provide a simple mechanism for monochromatization.

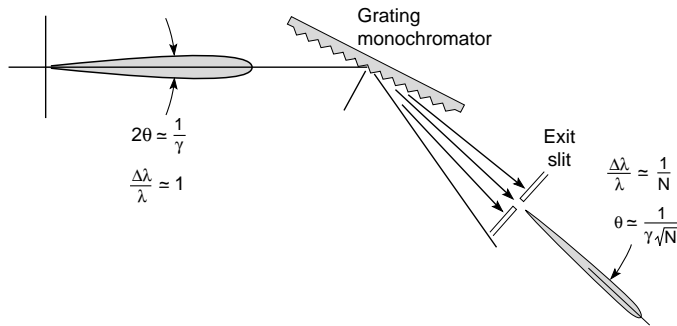


**FIGURE 5.14.** Illustration of a grating monochromator as used to filter undulator radiation to a “natural” spectral width  $1/N$ , and the concomitant cone narrowing to  $1/\gamma\sqrt{N}$  that occurs with a tightly constrained electron beam.

sets the monochromator for a “natural” bandwidth  $\Delta\lambda/\lambda$ , set by the number of oscillation periods,  $N$ , then one obtains the condition

$$\boxed{\frac{\Delta\lambda}{\lambda} = \frac{1}{N}} \quad (5.14)$$

which, when combined with Eq. (5.13), indicates that narrower bandwidth radiation occurs in a *concomitantly narrower “central” radiation cone* of half width

$$\boxed{\theta_{\text{cen}} \simeq \frac{1}{\gamma\sqrt{N}}} \quad (5.15)$$

This narrow undulator radiation cone implies an emission solid angle reduced by a factor  $1/N$ . These factors become very important when considering brightness and coherence (see Chapter 8).